

# SCIENTIFIC REPORTS



OPEN

## Electrochemical Energy Storage Application and Degradation Analysis of Carbon-Coated Hierarchical NiCo<sub>2</sub>S<sub>4</sub> Core-Shell Nanowire Arrays Grown Directly on Graphene/Nickel Foam

Received: 11 August 2015  
Accepted: 30 December 2015  
Published: 01 February 2016

Rujia Zou<sup>1,2</sup>, Muk Fung Yuen<sup>2</sup>, Li Yu<sup>1</sup>, Junqing Hu<sup>1</sup>, Chun-Sing Lee<sup>2</sup> & Wenjun Zhang<sup>2</sup>

We developed a new electrode comprising thin carbon layer coated hierarchical NiCo<sub>2</sub>S<sub>4</sub> core-shell nanowire arrays (NiCo<sub>2</sub>S<sub>4</sub>@C CSNAs) on graphene/Ni foam (Ni@G) substrates. The electrode showed outstanding electrochemical characteristics including a high specific capacitance of 253 mAh g<sup>-1</sup> at 3 A g<sup>-1</sup>, high rate capability of 163 mAh g<sup>-1</sup> at 50 A g<sup>-1</sup> (~64.4% of that at 3 A g<sup>-1</sup>), and long-term cycling stability with a capacity retention of 93.9% after 5000 cycles. Comparative studies on the degradation of hierarchical NiCo<sub>2</sub>S<sub>4</sub> CSNA electrodes with and without carbon coatings revealed that the morphology pulverization, structural separation at core/shell interface, and irretrievably chemical composition change of NiCo<sub>2</sub>S<sub>4</sub> CSNAs electrode are major factors that deteriorate the electrochemical performance of the electrodes without carbon coating. The favorable roles of carbon coatings on hierarchical NiCo<sub>2</sub>S<sub>4</sub> CSNAs were further clarified: (1) serving as a physical buffering layer that suppresses the structural breakdown; (2) retarding the chemical composition conversion of the NiCo<sub>2</sub>S<sub>4</sub> CSNAs; and (3) providing extra path for charge transition in addition to the NiCo<sub>2</sub>S<sub>4</sub> core nanowires. Understanding of the degradation mechanisms and the significance of the surface carbon coatings would provide useful guidelines for the design of new electrode materials for high-performance electrochemical devices.

With the rapid development of portable devices, green energy harvesting, and electric automobiles, safe energy storage devices with improved power and energy densities are becoming increasingly important. Electrochemical devices are very promising energy storage devices, due to their short charging time, high power densities, and long lifespans<sup>1,2</sup>. Among all these power sources, nanostructured electrode batteries and supercapacitors are the paradigm devices as they are promising to deliver power source with both high energy and power densities. The increasing applications of electrochemical devices in electronic devices and industries require on further improvement of the energy density, rate capability, safety, and durability of electrodes, which to a large extent rely on the development of new electrode materials and novel electrode structures. Transition metal oxides (MOs such as RuO<sub>2</sub>, MnO<sub>2</sub>, NiO, CoO) and sulfides (MSs such as CoS, NiS, WS<sub>2</sub> etc.) from an important group of electrode materials due to their abundant reversible redox reactions, high theoretical capacity, and long cycle life<sup>3–12</sup>. Recently, the ternary cobalt nickel sulfides (NiCo<sub>2</sub>S<sub>4</sub>) has drawn great research interest because of their intriguing advantages over the binary MOs and MSs<sup>2,13,14</sup>. For instance, NiCo<sub>2</sub>S<sub>4</sub> have an electrical conductivity of at least four orders of magnitude higher than that of either nickel oxides/sulfides or cobalt oxides/sulfides. High electrical conductivity could decrease the charge transfer resistance of the electrodes, and thus leading to increased power

<sup>1</sup>State Key Laboratory for Modification of Chemical Fibers and Polymer Materials, College of Materials Science and Engineering, Donghua University, Shanghai 201620, China. <sup>2</sup>Center of Super-Diamond and Advanced Films (COSDAF), Department of Physics and Materials Science, City University of Hong Kong, Hong Kong. Correspondence and requests for materials should be addressed to J.H. (email: hu.junqing@dhu.edu.cn) or W.Z. (email: apwjzh@cityu.edu.hk)

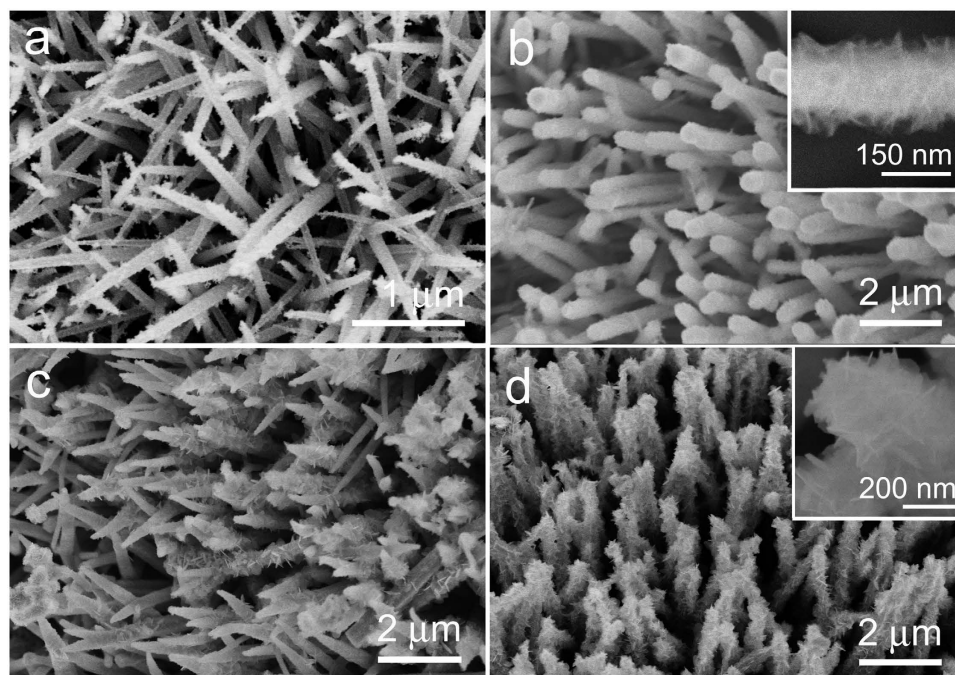


**Figure 1.** SEM images of the nanowire arrays obtained for different sulfurization time: (a) 12 h, (b) 24 h, (c) 36 h and (d) 48 h. Insets in (b,d) show the magnified images of hierarchical NiCo<sub>2</sub>S<sub>4</sub> CSNAs after sulfurization for 24 and 48 h, respectively.

density<sup>15,16</sup>. In addition, with the contributions from both nickel and cobalt ions, NiCo<sub>2</sub>S<sub>4</sub> are expected to offer richer redox reactions than the binary sulfides and oxides and thus increased capacity.

Various NiCo<sub>2</sub>S<sub>4</sub> nanostructures, including nanoparticles<sup>17,18</sup>, nanosheets<sup>19,20</sup>, nanotubes<sup>21</sup>, and microspheres<sup>22</sup>, have been synthesized. A common approach to apply these NiCo<sub>2</sub>S<sub>4</sub> nanostructures as electrodes in electrochemical devices is to mix them with polymeric binder and carbon black and press the mixture onto current collectors. However, the use of conductive additive and binder inevitably increases the undesirable interparticle resistance which decreases the efficiency of electron transport among active materials<sup>23,24</sup>. Recently, it was shown that direct growth of NiCo<sub>2</sub>S<sub>4</sub> nanowire arrays on metallic substrates could overcome the drawbacks from mixing active materials with conductive additive and binder, and led to improved capacity and cyclic stability<sup>25,26</sup>. Though NiCo<sub>2</sub>S<sub>4</sub> is important electrode material from those reported<sup>17–22</sup>, so far the change of electrochemical reactions on the surface/inside of NiCo<sub>2</sub>S<sub>4</sub> materials has not been studied systematically. Compared with one dimensional (1D) nanostructure, three dimensional (3D) heterostructure will be able to more fully be present in the change of electrode materials during electrochemical reactions<sup>27–29</sup>. In this work, we synthesized for the first time a thin carbon layer coated three dimensional (3D) hierarchical NiCo<sub>2</sub>S<sub>4</sub> core-shell nanowire arrays (NiCo<sub>2</sub>S<sub>4</sub>@C CSNAs) directly on graphene-coated Ni (Ni@G) foam. In comparison with the NiCo<sub>2</sub>S<sub>4</sub> nanowire arrays on metallic substrates, the effective surface area of the active electrode materials was greatly increased, and thus the electrochemical performances of the electrode was significantly improved, e.g., a high specific capacitance of 253 mAh g<sup>-1</sup> at 3 A g<sup>-1</sup>, high rate capability of 163 mAh g<sup>-1</sup> at 50 A g<sup>-1</sup> (~64.4% of that at 3 A g<sup>-1</sup>), and long-term cycling stability with a capacity retention of 93.9% after 5000 cycles. We further studied comparatively the degradation mechanisms of hierarchical NiCo<sub>2</sub>S<sub>4</sub> CSNAs electrodes with and without carbon coatings, and revealed favorable roles of carbon coatings in maintaining the structural integrity and chemical composition of the hierarchical NiCo<sub>2</sub>S<sub>4</sub> CSNAs during charge/discharge cycles.

## Results

The hierarchical NiCo<sub>2</sub>S<sub>4</sub> CSNAs were synthesized by hydrothermal method followed by sulfurization treatment (see the Supplementary Information I for Experimental details). Ni@G foams were used as substrates (Figure S1), and graphene was pre-coated on Ni foam to protect it which would otherwise become fragile during the sulfurization. For the synthesis of hierarchical NiCo<sub>2</sub>S<sub>4</sub> CSNAs, the Ni@G foam was first immersed into an aqueous solution containing Ni<sup>2+</sup>, Co<sup>2+</sup> and urea, and the (Ni, Co) hydroxide nanowire arrays were grown uniformly on the surface of Ni@G foam, as shown in Figure S2. Then, the (Ni, Co) hydroxide precursor nanowire arrays were converted to highly-ordered hierarchical NiCo<sub>2</sub>S<sub>4</sub> CSNAs via a facile sulfurization. Finally, the samples were annealed at 320 °C in Ar gas to get crystallized NiCo<sub>2</sub>S<sub>4</sub> CSNAs. As shown in Fig. 1a, the NiCo<sub>2</sub>S<sub>4</sub> nanowires on Ni@G foam possessed an average diameter of ~70 nm and length up to ~6 μm, and their surfaces were relatively smooth after sulfurization for 12 h. After sulfurization for 24 h, the NiCo<sub>2</sub>S<sub>4</sub> nanowires still remained the array structure, but the surface of nanowires became rough, as shown in Fig. 1b. Enlarged SEM image (inset in Fig. 1b) reveals that the nanowire surface was uniformly covered by clumps (a mat) of NiCo<sub>2</sub>S<sub>4</sub> nanosheets (as confirmed by XRD and HRTEM observations below), forming a core-shell hierarchical nanostructure. As the sulfurization

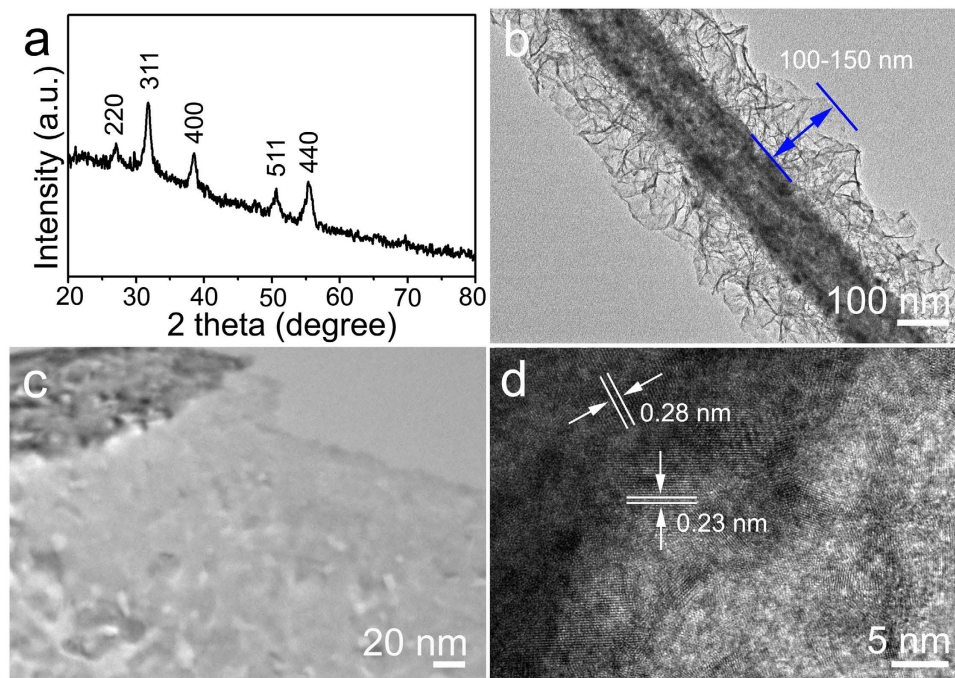


**Figure 2. Characterization of the hierarchical NiCo<sub>2</sub>S<sub>4</sub> core-shell nanowires.** (a) XRD pattern of the hierarchical NiCo<sub>2</sub>S<sub>4</sub> core-shell nanowires scratched from Ni@G foam. (b) TEM image of the hierarchical NiCo<sub>2</sub>S<sub>4</sub> core-shell nanowire, (c) Enlarged TEM view and (d) HRTEM image of the joint area between NiCo<sub>2</sub>S<sub>4</sub> nanowire and nanosheet.

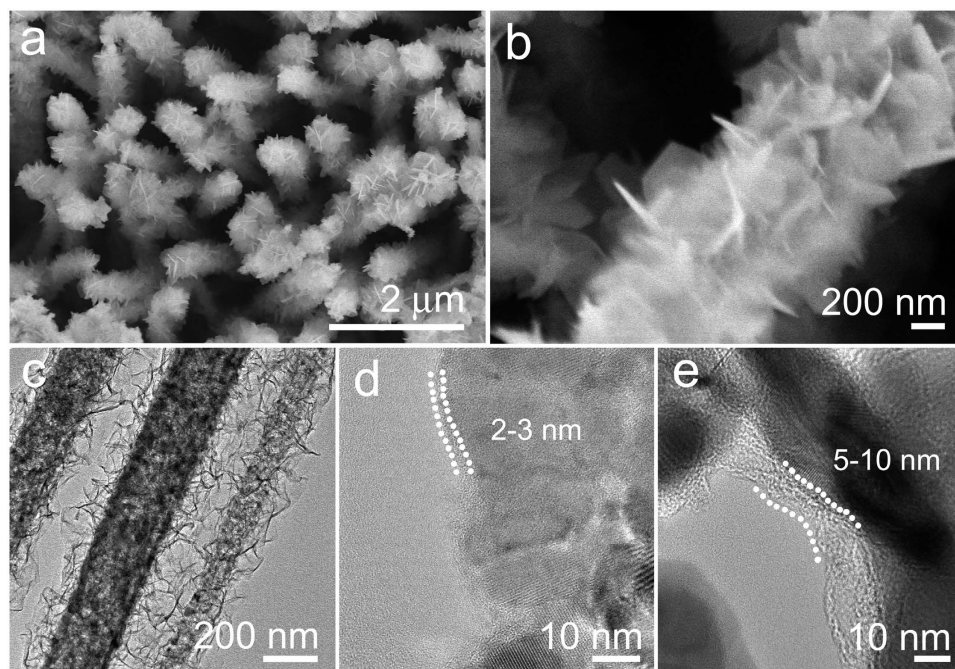
was prolonged to 36 h, the size of NiCo<sub>2</sub>S<sub>4</sub> nanosheets increased. However, not all NiCo<sub>2</sub>S<sub>4</sub> nanowires were covered by nanosheets. The uniform and large-scale NiCo<sub>2</sub>S<sub>4</sub> CSNAs on Ni@G foam were obtained after sulfuration for 48 h, as shown in Fig. 1d. Enlarged SEM image inset Fig. 1d reveals that ultrathin NiCo<sub>2</sub>S<sub>4</sub> nanosheets have a length of ~200 nm and a thickness of ~8 nm.

Figure 2a shows XRD pattern of the as-synthesized hierarchical NiCo<sub>2</sub>S<sub>4</sub> CSNAs scratched from Ni@G foam after sulfuration for 48 h. The diffraction peaks at 26.8°, 31.6°, 38.3°, 50.5° and 55.3° were indexed to the 220, 311, 400, 511, and 440 planes of the cubic NiCo<sub>2</sub>S<sub>4</sub> with reference to the standard diffraction pattern of NiCo<sub>2</sub>S<sub>4</sub> (Joint Committee on Powder Diffraction Standards (JCPDS) No. 20-0782). No other diffraction peaks were observed, verifying the formation of phase-pure NiCo<sub>2</sub>S<sub>4</sub>. The morphology and structure of hierarchical NiCo<sub>2</sub>S<sub>4</sub> CSNAs after sulfuration for 48 h were further investigated by using TEM. Consistent with the SEM observations above, the low-magnification TEM images (Fig. 2b and Figure S3) confirm the formation of uniform core-shell hierarchical structure with the NiCo<sub>2</sub>S<sub>4</sub> hollowed nanowire as core and NiCo<sub>2</sub>S<sub>4</sub> nanosheets (height up to ~100–150 nm) as shell. Interestingly, it is noted that all of the NiCo<sub>2</sub>S<sub>4</sub> core nanowires are mesoporous structure which is resulted from the replacement of O<sup>2-</sup> by S<sup>2-</sup> through sulfuration process<sup>30</sup>. The mesopores with a size ranging from 2 to 8 nm are uniformly distributed in the nanowires and nanosheets (Fig 2b,c), implying that the sulfuration processes homogeneously in the bulk of nanowires. HRTEM image in Fig. 2d further verified the crystal characteristics of NiCo<sub>2</sub>S<sub>4</sub> nanostructures. As denoted in this figure, the interplane distances were measured to be 0.28 nm and 0.23 nm, which correspond to the *d*-spacing of (311) and (400) planes of cubic NiCo<sub>2</sub>S<sub>4</sub>, respectively. The TEM observations verified that the hierarchical nanostructure is composed of the same electrochemical materials in core and shell, wherein both the nanowire core and the nanosheets shell could contribute to electrochemical reactions for energy storage. Moreover, the hierarchical NiCo<sub>2</sub>S<sub>4</sub> core-shell nanowires are featured with open spaces between shell nanosheets, which allow access of electrolyte to both core and shell surfaces and leads to improved electrochemical performance of active materials.

The surface area and porosity of hierarchical NiCo<sub>2</sub>S<sub>4</sub> CSNAs scratched from Ni@G foam were examined with adsorption-desorption experiment using Brunauer-Emmett-Teller (BET) method (Figure S4). Following the Barrett-Joyner-Halenda (BJH) method, NiCo<sub>2</sub>S<sub>4</sub> core-shell nanowires exhibited a pore size distribution ranging from 4 to 8 nm, which is consistent with the TEM observation in Fig. 2c. The specific surface area of hierarchical NiCo<sub>2</sub>S<sub>4</sub> core-shell nanowires was calculated to be 84.9 m<sup>2</sup>/g, which is significantly higher than those of the other NiCo<sub>2</sub>S<sub>4</sub> nanostructures reported in literatures<sup>18,19,31,32</sup>. A high specific surface area of active materials enables the efficient contact with electrolyte and increases the numbers of electroactive for charge storage and delivery.

The performance of electrochemical electrodes is known to depend strongly on the specific surface area and a well the electrical conductivity of the active materials<sup>1,2</sup>. In this work, the electric conductivity of an individual hierarchical NiCo<sub>2</sub>S<sub>4</sub> core-shell nanowire was measured *in situ* in TEM using a specially design holder (Nanofactory Instruments AB). The experimental setup is sketched in Figure S5a, and the other details have been reported in our previous work<sup>33,34</sup>. The hierarchical NiCo<sub>2</sub>S<sub>4</sub> core-shell nanowire bridged Au tip and Pt probe by precisely adjusting Pt probe using a piezo-driven manipulator, as shown in Figure S5b. For comparison, a





**Figure 3. Characterization of the hierarchical NiCo<sub>2</sub>S<sub>4</sub>@C CSNAs.** (a,b) SEM images of the hierarchical NiCo<sub>2</sub>S<sub>4</sub>@C CSNAs after carbon coating by hydrothermal reaction for 3h. (c) TEM image of the carbon-coated hierarchical NiCo<sub>2</sub>S<sub>4</sub>@C CSNAs after hydrothermal deposition for 3h. HRTEM images of hierarchical NiCo<sub>2</sub>S<sub>4</sub>@C CSNAs samples with carbon layers deposited by hydrothermal reaction for: (d) 3 h and (e) 8 h.

NiCo<sub>2</sub>O<sub>4</sub> nanowire without nanosheets shell was also measured using the same method (inset Figure S5b, see the Supplementary Information II for Experimental details). The corresponding *I*-*V* curves were shown in Figure S5c. Both of the voltage range from -1.0 to 1.0 V, the current value of hierarchical NiCo<sub>2</sub>S<sub>4</sub> core-shell nanowire varies from ~ -97.2 to 84.4 μA, while the current of NiCo<sub>2</sub>O<sub>4</sub> nanowire varies from ~ -0.39 to 0.35 μA. Thus, the electrical conductivity of the NiCo<sub>2</sub>S<sub>4</sub> core-shell nanowire is over 300 times higher than that of NiCo<sub>2</sub>O<sub>4</sub> nanowire, and about 4–5 orders of magnitude higher than those of metal oxides and sulfides in our previous work<sup>35,36</sup>.

A layer of carbon shell was deposited onto the surface of hierarchical NiCo<sub>2</sub>S<sub>4</sub> CSNAs by hydrothermal method. As shown in Fig. 3a, the hierarchical NiCo<sub>2</sub>S<sub>4</sub> CSNAs retained their morphology well after reaction for 3 h (see the Supplementary Information I for Experimental details). Enlarged SEM image in Fig. 3b reveals that the thickness of NiCo<sub>2</sub>S<sub>4</sub> nanosheets is increased to 10–12 nm after carbon coating. Agreeing with the SEM observations, the low-magnification TEM image in Fig. 3c also demonstrates that the NiCo<sub>2</sub>S<sub>4</sub> nanowires still maintain the core-shell structure with the nanowire cores uniformly covered by NiCo<sub>2</sub>S<sub>4</sub>. As further verified by the HRTEM image in Fig. 3d, a thin carbon layer shell with a thickness of 2–3 nm was deposited over the surface of hierarchical NiCo<sub>2</sub>S<sub>4</sub> CSNAs. The thickness of carbon layer could be controlled by reaction time, and it increased to 4–8 nm after reaction for 8 h (Fig. 3e).

The electrochemical performance of hierarchical NiCo<sub>2</sub>S<sub>4</sub>@C CSNAs on Ni@G foam was studied in a standard three-electrode configuration using 1.0 M KOH electrolyte. The control experiments on reference samples of hierarchical NiCo<sub>2</sub>S<sub>4</sub> CSNAs and NiCo<sub>2</sub>S<sub>4</sub> nanowire arrays (NAs) on Ni@G foams were also performed (see the Supplementary Information III for Experimental details and Figure S6). Because the 4–8 nm thick carbon layer restrain the ions in electrolyte to penetrate through it and react with the NiCo<sub>2</sub>S<sub>4</sub> CSNAs and leads to poor electrochemical performance (Figure S7), the following tests were conducted on the hierarchical NiCo<sub>2</sub>S<sub>4</sub>@C CSNAs with a thin carbon layer of 2–3 nm. Figure 4a presents the cyclic voltammetry (CV) curves of hierarchical NiCo<sub>2</sub>S<sub>4</sub>@C CSNAs electrode at different scan rates of 5, 10, 20, 30, 40 and 50 mV s<sup>-1</sup> in a potential window of -0.2–0.6 V. The redox current increased with the increase of scan rate from 5 to 50 mV s<sup>-1</sup>, and the oxidation and reduction peaks shifted toward higher and lower potentials, respectively, resulting in an enlarged potential separation. The CV curves of hierarchical NiCo<sub>2</sub>S<sub>4</sub> CSNAs and NiCo<sub>2</sub>S<sub>4</sub> NAs electrodes displayed the same tendency at different scan rates (Figure S8a), which suggests the same redox mechanism as that of hierarchical NiCo<sub>2</sub>S<sub>4</sub>@C CSNAs. However, at the same scan rate, the NiCo<sub>2</sub>S<sub>4</sub>@C CSNAs electrode has obviously a much larger integrated area than those of NiCo<sub>2</sub>S<sub>4</sub> CSNAs and NiCo<sub>2</sub>S<sub>4</sub> NAs electrodes, which indicates that the hierarchical NiCo<sub>2</sub>S<sub>4</sub>@C CSNAs electrode has a higher capacity. We also studied the CV characteristics of pure Ni@G foam, as shown in Figure S9. It was revealed that the pure Ni@G foam exhibited a much low capacity, indicating that the Ni@G foam had negligible contribution to the overall capacity of hierarchical NiCo<sub>2</sub>S<sub>4</sub>@C CSNAs electrode.

The galvanostatic charge-discharge (CD) tests of NiCo<sub>2</sub>S<sub>4</sub>@C CSNAs, NiCo<sub>2</sub>S<sub>4</sub> CSNAs and NiCo<sub>2</sub>S<sub>4</sub> NAs were performed in a potential window between 0 and 0.45 V at current densities ranging from 3 to 50 A g<sup>-1</sup>, as shown in Fig. 4b and Fig. S8. While close observation of the CV and CD curves of NiCo<sub>2</sub>S<sub>4</sub>@C CSNAs and NiCo<sub>2</sub>S<sub>4</sub> CSNAs electrodes suggested both capacitive effect and ion-diffusion effect for the energy storage, further analysis

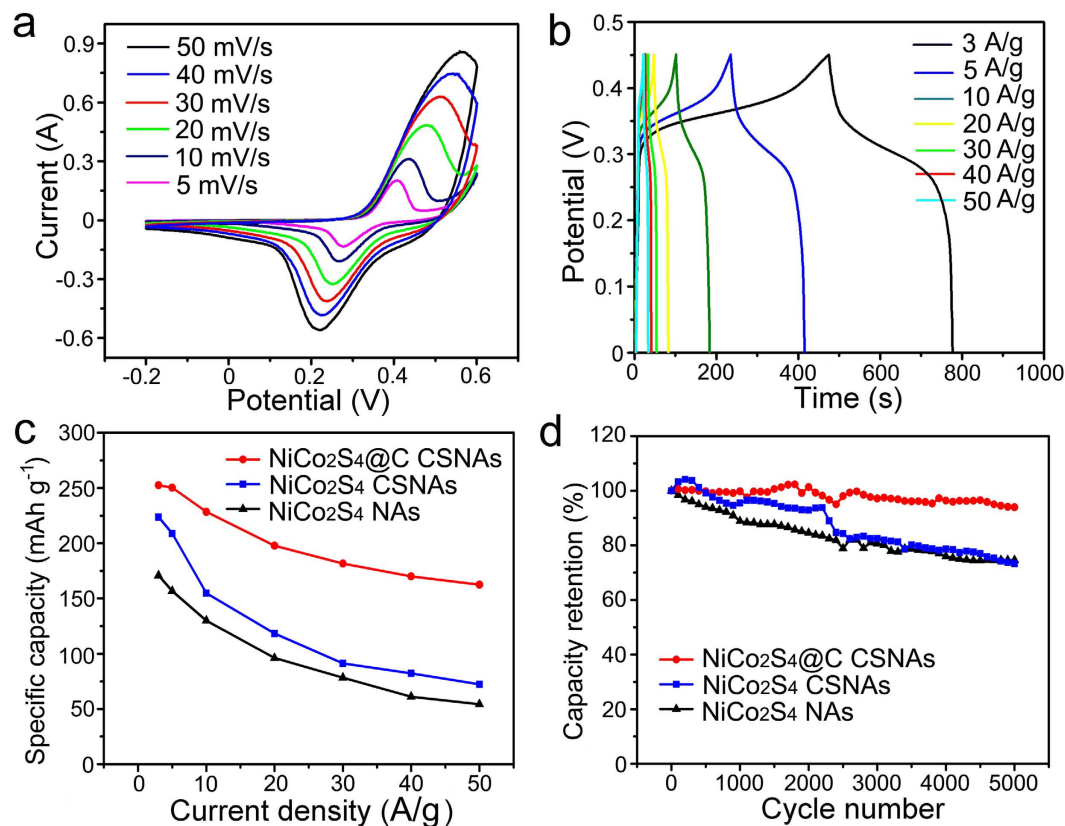


**Figure 4.** Electrochemical properties of  $\text{NiCo}_2\text{S}_4@C$  CSNAs,  $\text{NiCo}_2\text{S}_4$  CSNAs and  $\text{NiCo}_2\text{S}_4$  NAs electrodes in 1 M KOH aqueous solution at room temperature. (a) The CV curves of  $\text{NiCo}_2\text{S}_4@C$  CSNAs electrode at different scan rates. (b) The CD curves of  $\text{NiCo}_2\text{S}_4@C$  CSNAs electrode at different current densities. (c) Specific capacities of  $\text{NiCo}_2\text{S}_4@C$  CSNAs (red curve),  $\text{NiCo}_2\text{S}_4$  CSNAs (blue curve) and  $\text{NiCo}_2\text{S}_4$  NAs (black curve) electrodes at different current densities. (d) Cycling properties of  $\text{NiCo}_2\text{S}_4@C$  CSNAs (red curve),  $\text{NiCo}_2\text{S}_4$  CSNAs (blue curve) and  $\text{NiCo}_2\text{S}_4$  NAs (black curve) electrodes at a scan rate of  $50 \text{ mVs}^{-1}$  in 5000 cycles.

on the dependence of the current ( $i$ ) with the sweep rate ( $v$ ) at a fixed potential in reduction processes verified that they are closer to the battery-type materials (Figure S10)<sup>37–39</sup>. So, in order to obtain real and accurate values of the energy storage, the capacities were calculated based on the battery equation (unit,  $\text{mAh g}^{-1}$ ). According to previously reported<sup>40</sup>, the specific capacity values of the electrode materials are calculated from the galvanostatic discharge curves at various current densities. The specific capacity of  $\text{NiCo}_2\text{S}_4@C$  CSNAs was calculated to be 253, 250, 228, 198, 182, 170, and  $163 \text{ mAh g}^{-1}$  at current densities of 3, 5, 10, 20, 30, 40, and  $50 \text{ A g}^{-1}$ , respectively, as shown in Fig. 3c (red curve). The specific capacity of  $\text{NiCo}_2\text{S}_4$  CSNAs and  $\text{NiCo}_2\text{S}_4$  NAs electrodes at different current densities were also evaluated, as depicted by blue and black curves, respectively, in Fig. 4c. The specific capacity of hierarchical  $\text{NiCo}_2\text{S}_4@C$  CSNAs electrode is apparently higher than those of  $\text{NiCo}_2\text{S}_4$  CSNAs and  $\text{NiCo}_2\text{S}_4$  NAs electrodes for each current density. As the current densities increased from 3 to  $50 \text{ A g}^{-1}$ , the rate capability of  $\text{NiCo}_2\text{S}_4@C$  CSNAs,  $\text{NiCo}_2\text{S}_4$  CSNAs and  $\text{NiCo}_2\text{S}_4$  NAs electrodes were reduced to 64.4%, 32.3% and 31.7%, respectively, of their original values, indicating that  $\text{NiCo}_2\text{S}_4@C$  CSNAs electrode has best rate capability. As a result, at the current density of  $50 \text{ A g}^{-1}$ , the specific capacity of the  $\text{NiCo}_2\text{S}_4@C$  CSNAs  $\sim 2.3$  times higher than that of the is  $\text{NiCo}_2\text{S}_4$  CSNAs ( $163 \text{ mAh g}^{-1}$  vs.  $72 \text{ mAh g}^{-1}$ ). The cycling stability of  $\text{NiCo}_2\text{S}_4@C$  CSNAs,  $\text{NiCo}_2\text{S}_4$  CSNAs and  $\text{NiCo}_2\text{S}_4$  NAs electrodes were evaluated by repeated charge/discharge measurements at a scan rate of  $50 \text{ mVs}^{-1}$ , as shown in Fig. 4d. Interestingly, the overall loss of capacity of  $\text{NiCo}_2\text{S}_4@C$  CSNAs after 5000 cycles was less than 6.1%, i.e., the capacity retention of 93.9% over 5000 cycles, which is obviously superior to the  $\text{NiCo}_2\text{S}_4$  CSNAs (73.3%) and  $\text{NiCo}_2\text{S}_4$  NAs (74.6%) electrodes. The capacity retention of  $\text{NiCo}_2\text{S}_4$  NAs is slightly higher than that of hierarchical  $\text{NiCo}_2\text{S}_4$  CSNAs. On the one hand, high specific surface areas of active materials of  $\text{NiCo}_2\text{S}_4$  CSNAs enable the efficient contact with electrolyte, and increase the electroactive sites for redox reactions. On the other hand, compared with  $\text{NiCo}_2\text{S}_4$  NAs, hierarchical  $\text{NiCo}_2\text{S}_4$  CSNAs may result in structural change of nanosheets from nanowire cores more easily.

## Discussion

The above results revealed that the hierarchical  $\text{NiCo}_2\text{S}_4$  CSNAs electrodes have the following characteristics which have been demonstrated to be beneficial to improve the electrochemical performance<sup>27–29,41–45</sup>. First, both core and shell are active materials; and the 3D core-shell structure enables easy access of electrolyte. Therefore, both of them can effectively contribute to the capacity. Secondly, the hierarchical  $\text{NiCo}_2\text{S}_4$  CSNAs are highly conductive, which can provide “superhighways” for charge in the core-shell structure. The direct growth of  $\text{NiCo}_2\text{S}_4$



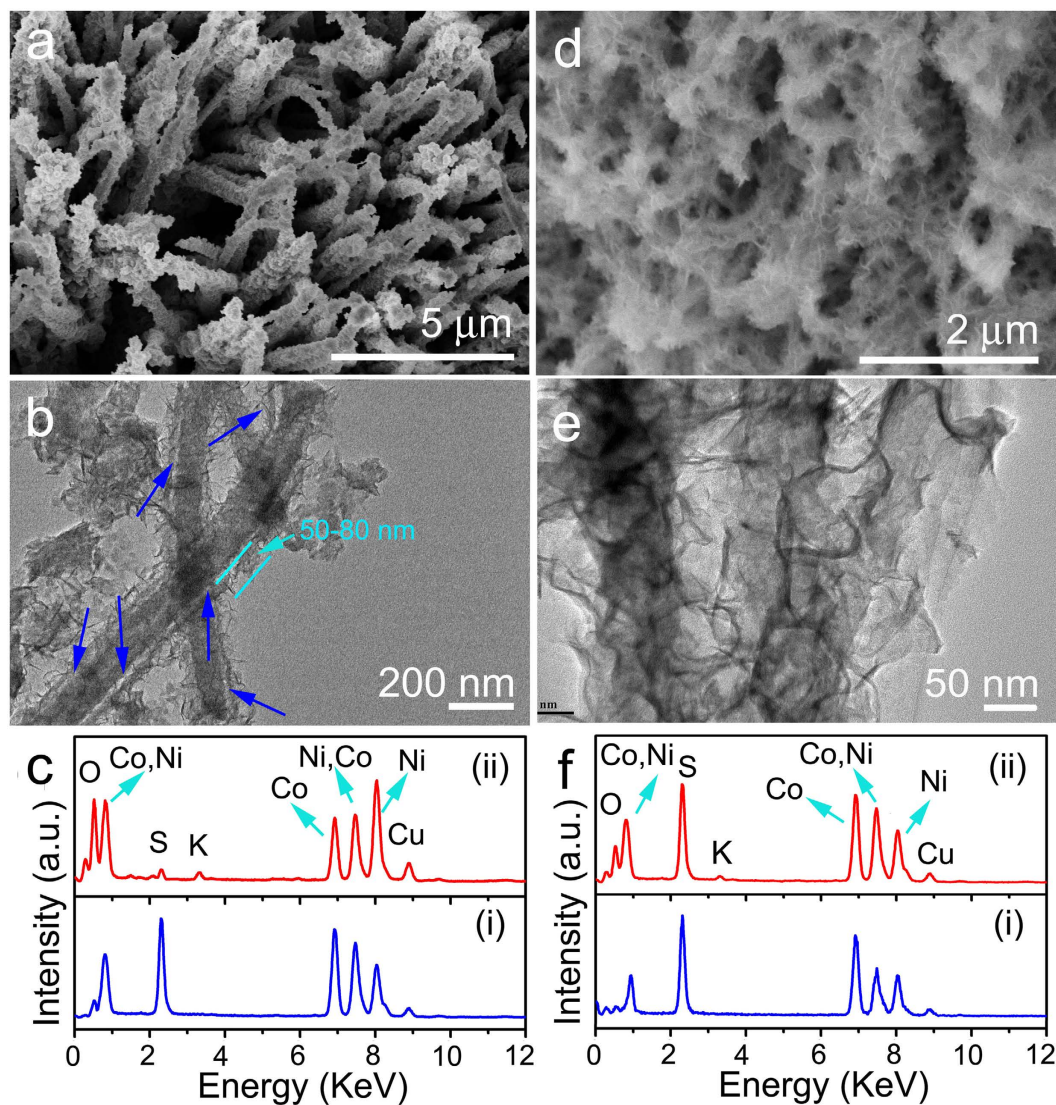


**Figure 5.** Characterization of the hierarchical  $\text{NiCo}_2\text{S}_4$  CSNAs and  $\text{NiCo}_2\text{S}_4@\text{C}$  CSNAs after charge/discharge for 5000 cycles at a scan rate of  $50 \text{ mV s}^{-1}$ . (a) SEM image, (b) TEM image, and (c) EDS pattern of the  $\text{NiCo}_2\text{S}_4$  CSNAs electrode after charge/discharge for 5000 cycles at a scan rate of  $50 \text{ mV s}^{-1}$ . (d) SEM image, (e) TEM image, and (f) EDS pattern of the  $\text{NiCo}_2\text{S}_4@\text{C}$  CSNAs electrode after charge/discharge for 5000 cycles at a scan rate of  $50 \text{ mV s}^{-1}$ .

nanoshells on  $\text{NiCo}_2\text{S}_4$  nanowires avoids the use of polymer binder/conductive additives and further guarantees the effective charge transport between them. Moreover, the  $\text{NiCo}_2\text{S}_4$  shells and  $\text{NiCo}_2\text{S}_4$  nanowires are mesoporous that increases the electroactive sites. Therefore, the hierarchical  $\text{NiCo}_2\text{S}_4$  CSNAs/ $\text{Ni}@G$  electrode has a comparable or even superior performance to the previously reported electrodes based on nickel/cobalt sulfide nanomaterials<sup>40</sup>. Surface carbon coating could significantly further improve the overall electrochemical properties, and made the hierarchical  $\text{NiCo}_2\text{S}_4@\text{C}$  CSNAs/ $\text{Ni}@G$  a very promising candidate for electrode applications.

In order to understand the degradation of electrochemical performance and beneficial role of surface carbon coating, we comparatively analyzed the variation of microstructure and chemical composition of the hierarchical  $\text{NiCo}_2\text{S}_4$  CSNAs with and without carbon coating after 5000 charge/discharge cycles. The structures of  $\text{NiCo}_2\text{S}_4$  CSNAs and  $\text{NiCo}_2\text{S}_4@\text{C}$  CSNAs electrodes after cycling at  $50 \text{ mV s}^{-1}$  were characterized by SEM and TEM. The morphology of the  $\text{NiCo}_2\text{S}_4$  CSNAs mainly retained their array structure, but the increased diameter and roughness of  $\text{NiCo}_2\text{S}_4$  nanowires after 5000 cycles, as shown in Fig. 5a and enlarged SEM image in Figure S11. However, TEM observation in Fig. 5b (more  $\text{NiCo}_2\text{S}_4$  core-shell nanowires in Figure S12) reveals that the  $\text{NiCo}_2\text{S}_4$  nanosheets were shortened to  $\sim 50\text{--}80 \text{ nm}$  in height, and shell nanosheets were detached from the core nanowires, forming a nanometer-scale gap between core and shell after 5000 cycles gaps, as denoted by the blue arrows. The breakdown of the hierarchical core-shell structure could possibly be caused by the repeated charge transfer through the core-shell interface during cycling processes which might induce uneven Joule heating and anisotropic volume expansion of nanowires and nanosheets of different geometric features.

The redox reactions during repeated charge/discharge processes may lead to dissolution of  $\text{NiCo}_2\text{S}_4$  into the electrolyte, and an irretrievably chemical composition change of the  $\text{NiCo}_2\text{S}_4$ . As shown by the EDS spectra for  $\text{NiCo}_2\text{S}_4$  CSNAs electrode before (i) and after (ii) 5000 cycles in Fig. 5c, the contents of Ni and S decreased, and O content increased drastically after cycling, suggesting the a variation of the chemical composition of  $\text{NiCo}_2\text{S}_4$  (Figure S13). Figure S14 shows representative CV curves of  $\text{NiCo}_2\text{S}_4$  CSNAs electrode in the voltage window of  $-0.2$  to  $0.6$  V at a scan rate of  $50 \text{ mV s}^{-1}$  for the 1<sup>st</sup>, 1000<sup>th</sup>, 2000<sup>th</sup>, 3000<sup>th</sup>, 4000<sup>th</sup> and 5000<sup>th</sup> cycles. The locations of the pair of current peaks for faradic oxidation/reduction reactions shifted obviously from the 1<sup>st</sup> to 5000<sup>th</sup> cycle, which further verifies a gradual change in the chemical composition of  $\text{NiCo}_2\text{S}_4$ . In the aqueous solution of KOH,  $\text{OH}^-$  ions and can serve as sources for the ion-exchange reaction to convert  $\text{NiCo}_2\text{S}_4$  to (Ni, Co) hydroxide.

The redox reactions occurred in both surface and inside of  $\text{NiCo}_2\text{S}_4$  nanosheets and nanowires, which may also result in the structural pulverization and detachment of nanosheet shell from nanowire core. The conversion of chemical composition from  $\text{NiCo}_2\text{S}_4$  to oxide and deterioration of the core-shell structure caused the increase of the resistance of hierarchical  $\text{NiCo}_2\text{S}_4$  CSNAs electrode after 5000 cycles as compared with that before cycling (as evidenced by EIS measurements in Figure S15). In addition, the specific surface area of hierarchical  $\text{NiCo}_2\text{S}_4$  core-shell nanowires was also reduced to  $38.9 \text{ m}^2/\text{g}$  after 5000 cycles (Figure S16), which is distinctly lower than that before charge/discharge processes ( $84.9 \text{ m}^2/\text{g}$ ). As a result of the gradual conversion of  $\text{NiCo}_2\text{S}_4$  to oxide with increased resistivity, the breakdown of the core-shell structure, and the reduced surface area of the  $\text{NiCo}_2\text{S}_4$  CSNAs electrode, the electrochemical performance of the  $\text{NiCo}_2\text{S}_4$  CSNAs electrode, including specific capacity, rate capability and cycling stability, deteriorated after charge/discharge cycles.

As the  $\text{NiCo}_2\text{S}_4$  CSNA electrodes were coated with a surface carbon layer, the  $\text{NiCo}_2\text{S}_4@\text{C}$  CSNAs still showed their hierarchical morphology after 5000 charge/discharge cycles (Fig. 5d). Interestingly, the TEM observation in Fig. 5e further revealed that the size of shell  $\text{NiCo}_2\text{S}_4$  nanosheets preserved and the  $\text{NiCo}_2\text{S}_4$  core-shell nanowires maintained their integrity without gaps formed at the core-shell interface. In a sharp contrast to the  $\text{NiCo}_2\text{S}_4$  CSNA electrodes, the EDS spectra for the  $\text{NiCo}_2\text{S}_4@\text{C}$  CSNAs before (i) and after (ii) 5000 cycles in Fig. 5e indicated that the electrode had its chemical composition almost unchanged with only a slight increase of oxygen content after long-term cycling (Figure S17). Correspondingly, the two strong peaks for the faradic oxidation/reduction reactions the CV curves showed only slight shift from 1<sup>st</sup> to 5000<sup>th</sup> CV curves (as denoted in Figure S18), which also verifies an unchanged composition of  $\text{NiCo}_2\text{S}_4@\text{C}$  CSNAs. Based on these observations, the surface carbon layer was demonstrated to play important roles in slowing down the degradation of the  $\text{NiCo}_2\text{S}_4@\text{C}$  CSNA electrode. First, it could serve as a physical buffer layer to suppress the structural alternation and counteract the pulverization of hierarchical  $\text{NiCo}_2\text{S}_4$  CSNAs. Second, it could function as a chemical blocking layer to retard the chemical composition conversion of the  $\text{NiCo}_2\text{S}_4$  CSNAs during cycling. Finally, it could also provide extra path for direct charge transport to current collector in addition to the conductive  $\text{NiCo}_2\text{S}_4$  core nanowires (Figure S19), which led to a lower resistivity of the hierarchical  $\text{NiCo}_2\text{S}_4@\text{C}$  CSNAs electrode than that of the  $\text{NiCo}_2\text{S}_4$  CSNAs electrode (Figure S20). Compared with the  $\text{NiCo}_2\text{S}_4$  CSNAs electrode (Figure S19a), the surface carbon layer in the  $\text{NiCo}_2\text{S}_4@\text{C}$  CSNAs electrode could also reduce repeated charge transfer through the core-shell interface, which could decrease the local Joule heat produced there and the resultant anisotropic volume expansions (-induced detachment of shell nanosheets from core nanowires) (Figure S19b). As a result,  $\text{NiCo}_2\text{S}_4@\text{C}$  CSNAs electrodes could have a much improved overall electrochemical performance including an increase of specific capacity by ( $253 \text{ mAh g}^{-1}$  vs.  $224 \text{ mAh g}^{-1}$  at  $3 \text{ A g}^{-1}$ , and  $163 \text{ mAh g}^{-1}$  vs.  $72 \text{ mAh g}^{-1}$  at  $50 \text{ A g}^{-1}$ ), the rate capability ( $64.4\%$  vs.  $32.3\%$ ) and cycling stability (retention of  $93.9\%$  vs.  $73.3\%$ ).

We have successfully synthesized the hierarchical  $\text{NiCo}_2\text{S}_4@\text{C}$  CSNAs directly on Ni@G foams using hydrothermal reactions followed by a sulfurization process. The hierarchical  $\text{NiCo}_2\text{S}_4@\text{C}$  CSNAs electrode exhibits exceptionally high specific capacity ( $253 \text{ mAh g}^{-1}$  at  $3 \text{ A g}^{-1}$ ), high rate capability ( $\sim 64.4\%$  retention from at  $3$  to  $50 \text{ A g}^{-1}$ ), and excellent cycling stability ( $6.1\%$  capacity loss after 5000 cycles at  $50 \text{ mVs}^{-1}$ ). By comparatively studying the degradation of hierarchical  $\text{NiCo}_2\text{S}_4$  CSNAs electrode with and without carbon coatings, we revealed that the morphology pulverization, structural separation at core/shell interface, and irretrievably chemical composition change of  $\text{NiCo}_2\text{S}_4$  CSNAs electrode during charge/discharge cycles are major factors that resulted in reduction of the specific capacity, deterioration of the rate capability and long-term cycling stability of the  $\text{NiCo}_2\text{S}_4$  CSNAs electrodes. The surface carbon coating was demonstrated to be able to improve drastically the electrochemical performance of the  $\text{NiCo}_2\text{S}_4$  CSNAs electrodes, which could serve as a physical buffering layer to suppress the structural breakdown, diminish the chemical composition conversion of the  $\text{NiCo}_2\text{S}_4$  CSNAs, and provide extra path for charge transition in addition to the  $\text{NiCo}_2\text{S}_4$  core nanowires. The understanding of the degradation mechanism of the core-shell nanostructured electrodes and as well the beneficial roles of surface carbon coating will be helpful for the design and fabrication of new electrodes for high-performance electrochemical devices.

## Methods

**Synthesis.** All chemicals were purchased from Sigma-Aldrich were used as received without further purification. The hierarchical  $\text{NiCo}_2\text{S}_4$  CSNAs, hierarchical  $\text{NiCo}_2\text{S}_4@\text{C}$  CSNAs and  $\text{NiCo}_2\text{O}_4$  NAs were synthesized on Ni@G foam using hydrothermal reactions followed by a simple sulfurization treatment. The detailed conditions, e.g. source materials, processing temperature, and time, are provided in Supplementary Information I, II and III. The loading weight of hierarchical  $\text{NiCo}_2\text{S}_4$  CSNAs and hierarchical  $\text{NiCo}_2\text{S}_4@\text{C}$  CSNAs was about  $3.4\text{--}3.6 \text{ mg cm}^{-2}$ .

**Characterization.** The as-synthesized products were characterized with a D/max-2550 PC X-ray diffractometer (XRD; Rigaku, Cu-K $\alpha$  radiation), a scanning electron microscope (SEM; S-4800), a transmission electron microscope (TEM; JEM-2100F) equipped with an energy dispersive X-ray spectrometer (EDX), and an X-ray photoelectron spectrometer (ESCALab MKII) with an excitation source of Mg-K radiation. The surface

area and pore size distribution of the products were determined by Brunauer-Emmett-Teller (BET) nitrogen adsorption-desorption and Barrett-Joyner-Halenda (BJH) methods (Micromeritics, ASAP2020). The electrical properties of samples were tested *in situ* by using a TEM-scanning tunneling microscope (TEM-STM) holder (commercialized by Nanofactory Instruments AB, Göteborg, Sweden), which was arranged within a 200 kV high resolution TEM (JEM-2100F) with beam-blank irradiation of a low illumination.

**Electrochemical measurements.** Electrochemical measurements were performed on an Autolab Electrochemical Workstation (PGSTAT302N) using a three electrode electrochemical cell and 1 M KOH as the electrolyte. The Ni@G foam supported electroactive materials (1 cm × 1 cm) were directly used as the working electrode. A saturated calomel electrode (SCE) was used as the reference electrode and a platinum (Pt) sheet was used as the counter electrode. All potentials were referred to the reference electrode. The specific capacity and current density were calculated based on the mass of these electroactive materials.

## References

- Wang, G. P., Zhang, L. & Zhang, J. J. A Review of Electrode Materials for Electrochemical Supercapacitors. *Chem. Soc. Rev.* **41**, 797–828 (2012).
- Augustyn, V., Simon, P. & Dunn, B. Pseudocapacitive Oxide Materials for High-rate Electrochemical Energy Storage. *Energy Environ. Sci.* **7**, 1597–1614 (2014).
- Hu, C. C., Chang, K. H., Lin, M. C. & Wu, Y. T. Design and Tailoring of the Nanotubular Arrayed Architecture of Hydrated RuO<sub>2</sub> for Next Generation Supercapacitors. *Nano Lett.* **6**, 2690–2695 (2006).
- Ma, R. H., Bando, Y. L., Zhang, Q. & Sasaki, T. Layered MnO<sub>2</sub> Nanobelts: Hydrothermal Synthesis and Electrochemical Measurements. *Adv. Mater.* **16**, 918–922 (2004).
- Singh, A. K., Sarkar, D., Khan, G. G. & Mandal, K. Hydrogenated NiO Nanoblock Architecture for High Performance Pseudocapacitor. *ACS Appl. Mater. Interfaces* **6**, 4684–4692 (2014).
- Zhu, Y. G. *et al.* Phase Transformation Induced Capacitance Activation for 3D Graphene-CoO Nanorod Pseudocapacitor. *Adv. Energy Mater.* **4**, 1301788 (2014).
- Peng, S. J. *et al.* MS<sub>2</sub> (M = Co and Ni) Hollow Spheres with Tunable Interiors for High-Performance Supercapacitors and Photovoltaics. *Adv. Funct. Mater.* **24**, 2155–2162 (2014).
- Xia, X. H. *et al.* Synthesis of Free-Standing Metal Sulfide Nanoarrays via Anion Exchange Reaction and Their Electrochemical Energy Storage Application. *Small* **10**, 766 (2014).
- Sun, C. C. *et al.* Phase-controlled synthesis of  $\alpha$ -NiS nanoparticles confined in carbon nanorods for High Performance Supercapacitors. *Sci. Rep.* **4**, 7054 (2014).
- Ratha, S. & Rout, C. S. Supercapacitor Electrodes Based on Layered Tungsten Disulfide-Reduced Graphene Oxide Hybrids Synthesized by a Facile Hydrothermal Method. *ACS Appl. Mater. Interfaces* **5**, 11427–11433 (2013).
- Cao, X. H., Yin, Z. Y. & Zhang, H. Three-Dimensional Graphene Materials: Preparation, Structures and Application in Supercapacitors. *Energy Environ. Sci.* **7**, 1850–1865 (2014).
- Rui, X. H., Tan, H. T. & Yan, Q. Y. Nanostructured Metal Sulfides for Energy Storage. *Nanoscale* **6**, 9889–9924 (2014).
- Zou, R. J. *et al.* Three-Dimensional Networked NiCo<sub>2</sub>S<sub>4</sub> Nanosheet Arrays/Carbon Cloth Anodes for High-Performance Lithium-Ion Batteries. *NPG Asia Materials* **7**, e195 (2015).
- Chen, H. C. *et al.* Highly Conductive NiCo<sub>2</sub>S<sub>4</sub> Urchin-Like Nanostructures for High-Rate Pseudocapacitors. *Nanoscale* **5**, 8879–8883 (2013).
- Hu, L. B. *et al.* Highly Conductive Paper for Energy-Storage Devices. *P. Natl. Acad. Sci. USA* **106**, 21490–21494 (2009).
- Frackowiak, E. & Béguin, F. Carbon Materials for the Electrochemical Storage of Energy in Capacitors. *Carbon* **39**, 937–950 (2001).
- Liu, Q., Jin, J. T. & Zhang, J. Y. NiCo<sub>2</sub>S<sub>4</sub>@graphene as a Bifunctional Electrocatalyst for Oxygen Reduction and Evolution Reactions. *ACS Appl. Mater. Interfaces* **5**, 5002–5008 (2013).
- Du, W. M. *et al.* One-Step Synthesis of CoNi<sub>2</sub>S<sub>4</sub> Nanoparticles for Supercapacitor Electrodes. *RSC Adv.* **4**, 6998–7002 (2014).
- Shen, L. F. *et al.* NiCo<sub>2</sub>S<sub>4</sub> Nanosheets Grown on Nitrogen-Doped Carbon Foams as an Advanced Electrode for Supercapacitors. *Adv. Energy Mater.* **5**, 1400977 (2015).
- Yang, J. Q. *et al.* Hierarchical porous NiCo<sub>2</sub>S<sub>4</sub> hexagonal plates: Formation via chemical conversion and application in high performance supercapacitors. *Electrochimica Acta* **144**, 16–21 (2014).
- Wan, H. Z. *et al.* NiCo<sub>2</sub>S<sub>4</sub> Porous Nanotubes Synthesis via Sacrificial Templates: High-Performance Electrode Materials of Supercapacitors. *CrystEngComm* **15**, 7649–7651 (2013).
- Zhang, Z. Y. *et al.* NiCo<sub>2</sub>S<sub>4</sub> Sub-Micron Spheres: An Efficient Non-Precious Metal Bifunctional Electrocatalyst. *Nanoscale* **6**, 3540–3544 (2014).
- Cong, S., Tian, Y. Y., Li, Q. W., Zhao, Z. G. & Geng, F. X. Single-Crystalline Tungsten Oxide Quantum Dots for Fast Pseudocapacitor and Electrochromic Applications. *Adv. Mater.* **26**, 4260–4267 (2014).
- Oh, P. *et al.* Superior Long-Term Energy Retention and Volumetric Energy Density for Li-rich Cathode Materials. *Nano Lett.* **14**, 5965–5972 (2014).
- Xiao, J. W., Wan, L., Yang, S. H., Xiao, F. & Wang, S. A. Design Hierarchical Electrodes with Highly Conductive NiCo<sub>2</sub>S<sub>4</sub> Nanotube Arrays Grown on Carbon Fiber Paper for High-Performance Pseudocapacitors. *Nano Lett.* **14**, 831–838 (2014).
- Chen, H. C. *et al.* *In Situ* Growth of NiCo<sub>2</sub>S<sub>4</sub> Nanotube Arrays on Ni Foam for Supercapacitors: Maximizing Utilization Efficiency at High Mass Loading to Achieve Ultrahigh Areal Pseudocapacitance. *J. Power Sources* **254**, 249–257 (2014).
- Tian, W. *et al.* Ni(OH)<sub>2</sub> Nanosheet@Fe<sub>2</sub>O<sub>3</sub> Nanowire Hybrid Composite Arrays for High-Performance Supercapacitor Electrodes. *Nano Energy* **2**, 754–763 (2013).
- Wang, X. *et al.* Cu/Li<sub>4</sub>Ti<sub>5</sub>O<sub>12</sub> Scaffolds as Superior Anodes for Lithium-Ion Batteries. *NPG Asia Materials* **7**, e171 (2015).
- Guan, H., Wang, X., Chen, S. M., Bando, Y. & Golberg, D. Coaxial Cu-Si@C Array Electrodes for High-Performance Lithium Ion Batteries. *Chem. Commun.* **47**, 12098–12100 (2011).
- Kung, C. W. *et al.* CoS Acicular Nanorod Arrays for the Counter Electrode of an Efficient Dye-Sensitized Solar Cell. *ACS Nano* **6**, 7016–7025 (2012).
- Zhang, Y. F. *et al.* Shape-Controlled Synthesis of NiCo<sub>2</sub>S<sub>4</sub> and Their Charge Storage Characteristics in Supercapacitors. *Nanoscale* **6**, 9824–9830 (2014).
- Peng, T. *et al.* Construction of Mass-Controllable Mesoporous NiCo<sub>2</sub>S<sub>4</sub> Electrodes for High Performance Supercapacitors. *J. Mater. Chem. A* **2**, 19376–19382 (2014).
- Liu, Q., Zou, R. J., Bando, Y., Golberg, D. & Hu, J. Q. Nanowires Sheathed Inside Nanotubes: Manipulation, Properties and Applications. *Prog. Mater. Sci.* **70**, 1–49 (2015).
- Zou, R. J. *et al.* Melting of Metallic Electrodes and Their Flowing Through a Carbon Nanotube Channel within a Device. *Adv. Mater.* **25**, 2693–2699 (2013).
- Zou, R. J. *et al.* High Detectivity Solar-Blind High-Temperature Deep-Ultraviolet Photodetector Based on Multi-Layered (100) Facet-Oriented  $\beta$ -Ga<sub>2</sub>O<sub>3</sub> Nanobelts. *Small* **10**, 1848–1856 (2014).



36. Zou, R. J., Yu, L., Zhang, Z. Y., Chen, Z. G. & Hu, J. Q. High-Precision, Large-Domain Three-Dimensional Manipulation of Nano-Materials for Fabrication Nanodevices. *Nanoscale Res. Lett.* **6**, 473 (2011).
37. Simon, P., Gogotsi, Y. & Dunn, B. Where Do Batteries End and Supercapacitors Begin? *Science* **343**, 1210–1211 (2014).
38. Conway, B. E. Transition from “Supercapacitor” to “Battery” Behavior in Electrochemical Energy Storage. *J. Electrochem. Soc.* **138**, 1539–1548 (1991).
39. Lindström, H. *et al.* Li<sup>+</sup> Ion Insertion in TiO<sub>2</sub> (Anatase). 2. Voltammetry on Nanoporous Films. *J. Phys. Chem. B* **101**, 7717–7722 (1997).
40. Xia, X. H. *et al.* Synthesis of Free-Standing Metal Sulfide Nanoarrays via Anion Exchange Reaction and Their Electrochemical Energy Storage Application. *Small* **10**, 766–773 (2014).
41. Zhou, W. J. *et al.* One-step synthesis of Ni<sub>3</sub>S<sub>2</sub> nanorod@Ni(OH)<sub>2</sub> nanosheet core-shell nanostructures on a three-dimensional graphene network for high-performance supercapacitors. *Energy Environ. Sci.* **6**, 2216–2221 (2013).
42. Guan, C. *et al.* Hollow Core-Shell Nanostructure Supercapacitor Electrodes: Gap Matters. *Energy Environ. Sci.* **5**, 9085–9090 (2012).
43. Xia, X. H. *et al.* High-Quality Metal Oxide Core/Shell Nanowire Arrays on Conductive Substrates for Electrochemical Energy Storage. *ACS Nano* **6**, 5531–5538 (2012).
44. Sun, J. Q. *et al.* 3D Core/Shell Hierarchies of MnOOH Ultrathin Nanosheets Grown on NiO Nanosheet Arrays for High-Performance Supercapacitors. *Nano Energy* **4**, 56–64 (2014).
45. Zou, R. J. *et al.* Dendritic Heterojunction Nanowire Arrays for High-Performance Supercapacitors. *Sci. Rep.* **5**, 7862 (2015).

## Acknowledgements

This work was financially supported by the National Natural Science Foundation of China (Grant Nos. 21171035, 51302035, and 51372213), the PhD Programs Foundation of the Ministry of Education of China (Grant Nos. 20110075110008 and 20130075120001), the Science and Technology Commission of Shanghai Municipality (Grant No. 13ZR1451200), the China Postdoctoral Science Foundation (Grant No. 2014M550203), and the Applied Research Grant of the City University of Hong Kong (ARG 9667111).

## Author Contributions

R.J.Z. and W.J.Z. designed and performed the experiments. R.J.Z., L.Y. and M.F.Y. prepared the samples and analyzed the data. R.J.Z., J.Q.H., C.S.L. and W.J.Z. participated in interpreting and analyzing the data. R.J.Z., M.F.Y. and W.J.Z. wrote the manuscript.

## Additional Information

**Supplementary information** accompanies this paper at <http://www.nature.com/srep>

**Competing financial interests:** The authors declare no competing financial interests.

**How to cite this article:** Zou, R. *et al.* Electrochemical Energy Storage Application and Degradation Analysis of Carbon-Coated Hierarchical NiCo<sub>2</sub>S<sub>4</sub> Core-Shell Nanowire Arrays Grown Directly on Graphene/Nickel Foam. *Sci. Rep.* **6**, 20264; doi: 10.1038/srep20264 (2016).



This work is licensed under a Creative Commons Attribution 4.0 International License. The images or other third party material in this article are included in the article's Creative Commons license, unless indicated otherwise in the credit line; if the material is not included under the Creative Commons license, users will need to obtain permission from the license holder to reproduce the material. To view a copy of this license, visit <http://creativecommons.org/licenses/by/4.0/>